Prediction of velocity statistics in three-dimensional multi-Gaussian hydraulic conductivity fields

Andreas Englert,[1] Jan Vanderborght,[1] and Harry Vereecken[1]

Received 2 February 2005; revised 1 December 2005; accepted 21 December 2005; published 22 March 2006.

[1] To study statistics of velocity fields in three-dimensional heterogeneous multi-Gaussian saturated hydraulic conductivity fields and the accuracy of their prediction, we performed high-resolution Monte Carlo (MC) analyses. The MC analyses included variances of the log hydraulic conductivity in the range of $0.5 \leq \sigma_Y^2 \leq 3.0$ and anisotropy ratios in the range of $0.017 \leq e \leq 1$. The statistics of the velocity fields from the MC analyses are compared with analytical solutions of the first- and second-order approximations of the stochastic flow equation. This paper shows that the second-order approximations fit significantly better to the univariate statistics of the Darcy velocity from the MC analyses. For isotropic cases the second-order approximations correspond fairly well to the univariate statistics of the velocity. For anisotropic cases the accordance is given only for the mean velocity and the variance of the transverse vertical component of the velocity. The MC analyses show that the spatial correlation of the velocity decreases more rapidly with increasing σ_Y^2. This was more pronounced for the anisotropic than for the isotropic case. The negative correlations, in absolute terms, of the transverse velocity components simultaneously decrease with increasing σ_Y^2. This is in contrast to the first-order approximation of the spatial correlations of the velocity. It is assumed that the discrepancies between approximate solutions of the stochastic flow equation and the results of the MC analyses are strongly dependent on the nonnormality of the probability density distributions of the velocity.

Citation: Englert, A., J. Vanderborght, and H. Vereecken (2006), Prediction of velocity statistics in three-dimensional multi-Gaussian hydraulic conductivity fields, *Water Resour. Res.*, *42*, W03418, doi:10.1029/2005WR004014.

1. Introduction

[2] It is well established that the transport of substances in groundwater is strongly determined by the spatial heterogeneity of the groundwater flow velocity, which is highly dependent on the heterogeneity of the hydraulic conductivity [e.g., *Mackay et al.*, 1986; *Leblanc et al.*, 1991; *Boggs et al.*, 1992; *Vereecken et al.*, 2000]. Therefore it is indispensable to incorporate effects of spatial heterogeneity in predictions of flow and transport in groundwater.

[3] Since it is impossible to determine the structure of an aquifer in a deterministic sense, based on point-scale information derived from borehole measurements, the heterogeneity of an aquifer is characterized in a geostatistical sense. As a consequence, research is aimed at linking geostatistical parameters of the hydraulic conductivity field with those of the Darcy velocity and head fields. In this field of research several techniques, each with its specific advantages, are described in the literature. In this study we focus on the evaluation of approximate solutions of the stochastic differential flow equation using Monte Carlo analyses, both based on multi-Gaussian log hydraulic conductivity fields.

[4] Over the last thirty years, stochastic flow equations were developed that quantify the effect of spatial heterogeneity of the hydraulic conductivity, K, on the Darcy velocity, $\vec{q}$, and total head, H. Perturbation approaches were applied to Darcy's law and the continuity equation in order to find closed form functions deriving the geostatistical parameters of $\vec{q}$ from those of the K [e.g., *Dagan*, 1989; *Gelhar*, 1993; *Zhang*, 2002; *Rubin*, 2003]. These functions are approximate solutions which were obtained after a truncation of the perturbated Darcy's law and continuity equation. Extensive work has been carried out on first-order approximations [e.g., *Gelhar and Axness*, 1983; *Dagan*, 1984; *Rubin and Dagan*, 1992; *Neuman and Orr*, 1993; *Russo*, 1995; *Hsu et al.*, 1996; *Bonilla and Cushman*, 2000], less attention has been paid to second-order approximations of the perturbated equations in two (2-D) [*Hsu et al.*, 1996], and three dimensions (3-D) [*Deng and Cushman*, 1995; *Hsu and Neuman*, 1997; *Deng and Cushman*, 1998]. The theoretical validity of the approximate solutions of the stochastic flow equation was established for small values of the variance of the logarithm of the hydraulic conductivity, σ_Y^2. The validity of these approximate solutions for large values of σ_Y^2 is in many cases unclear.

[5] In order to test the validity of the approximate solutions for higher σ_Y^2, Monte Carlo (MC) analyses are an appropriate tool. In MC analysis several realizations of the random space function, which characterizes the spatial variability of the hydraulic conductivity field, are generated. Subsequently the flow equation in these realizations is solved numerically. Statistical analysis of $\vec{q}$, including all of these realizations, allows for detailed study of the

[1]Agrosphere Institute (ICG IV), Institute of Chemistry and Dynamics of the Geosphere, Research Center Jülich, Jülich, Germany.

0043-1397/06/2005WR004014

Table 1. Three-Dimensional Monte Carlo Analyses on Velocities From Literature

Source	Preset K Statistics		Rating of the MC Analyses	
	Range of σ_Y^2	Range of e	Number of Elements	Number of Realizations
Ababou et al. [1989]	1.0–5.29	1	13×10^4	1
Tompson and Gelhar [1990]	1.0–5.29	1	12×10^4	1
Chin and Wang [1992]	0.1–1.5	1	12×10^4	92
Dykaar and Kitanidis [1992]	1–6.0	1	17×10^6	1
Neuman et al. [1992]	0.25–7.0	1	42.9×10^3	500
Burr et al. [1994]	0.04	0.18	11×10^4	25
Naff et al. [1998a]	0.09–0.9	0.05–0.26	90×10^4	900
Present study	0.5–3.0	0.017–1.0	12×10^6	10

univariate and spatial statistics of the components of the velocity vector in terms of ensemble parameters. In the following, the mean flow direction is denoted as longitudinal direction, *l* direction. Perpendicular to the mean flow direction are the transverse horizontal, *th* direction, and the transverse vertical direction, *tv* direction. Furthermore $e = \frac{\lambda_v}{\lambda_h}$ is the anisotropy ratio with λ_v being the correlation length in *tv* direction and λ_h being the correlation length in *l* and *th* directions, which are defined to be equal.

[6] For 2-D isotropic hydraulic conductivity fields it was shown that the first-order approximation of the effective hydraulic conductivity is correct [e.g., *Matheron*, 1967; *Janković et al.*, 2003b]. Using a MC approach, it was also shown for 2-D isotropic hydraulic conductivity fields [e.g., *Bellin et al.*, 1992; *Salandin and Fiorotto*, 1998; *Hassan et al.*, 1998] that the estimation of the flow velocity variance is accurate up to $\sigma_Y^2 = 1$ using first order approximation and up to $\sigma_Y^2 = 2$ using second-order approximation. Moreover the first order approximation of the correlation of the flow velocity is independent of σ_Y^2 and exact for $\sigma_Y^2 \ll 1$. In addition it was found that for higher σ_Y^2 the correlation lengths of the flow velocity decrease with increasing σ_Y^2.

[7] The results of the 2-D simulations and approximations of flow in a heterogeneous conductivity field can be extrapolated to real 3-D flow and conductivity fields but only in a qualitative sense [e.g., *Russo*, 1998]. Because of the increase of the numerical demands with the increase of the dimensionality of the flow problem, only a few studies report on the validity of approximate solutions of the stochastic differential flow equation in 3-D cases (see Table 1).

[8] For 3-D isotropic hydraulic conductivity fields it was shown that first-order estimates of the mean Darcy velocity are valid up to $\sigma_Y^2 \leq 1$ and valid up to at least $\sigma_Y^2 = 7$ for second-order estimates [*Ababou et al.*, 1989; *Tompson and Gelhar*, 1990; *Chin and Wang*, 1992; *Dykaar and Kitanidis*, 1992; *Neuman et al.*, 1992]. The first-order estimates of the covariances of the Darcy velocity components are valid for $\sigma_Y^2 \leq 0.5$. The validity of second-order approximations estimating the covariance of the velocity is still an unresolved issue.

[9] For 3-D anisotropic hydraulic conductivity fields it was shown that the first-order approximation of the mean velocity is only valid for $\sigma_Y^2 \leq 0.5$ at $e \geq 0.07$ [*Burr et al.*, 1994; *Naff et al.*, 1998a]. Estimates of the mean velocity by second-order approximation are accurate at least up to $\sigma_Y^2 = 0.9$ at $e = 0.05$. The validity for $\sigma_Y^2 > 0.9$ is an unsettled topic. It was also shown that for $\sigma_Y^2 \leq 0.18$ and $e = 0.04$, first-order estimates of the covariance of the longitudinal velocity component in *l* direction fit fairly well to results from MC analyses. The validity of first- and second-order estimates of the covariances of the transverse velocity components and of the longitudinal component at $\sigma_Y^2 \geq 0.18$ for anisotropic media is still an unresolved topic. This is of particularly interest, since first- and second-order approximations deviate stronger for larger anisotropy and larger σ_Y^2 [*Deng and Cushman*, 1995; *Hsu and Neuman*, 1997; *Deng and Cushman*, 1998].

[10] The objective of this paper is to systematically evaluate the effect of e and σ_Y^2 in 3-D hydraulic conductivity fields on the flow field statistics and compare them with first- and second-order approximations. Results of MC analyses will be presented for $0.5 \leq \sigma_Y^2 \leq 3.0$ and $0.017 \leq e \leq 1$. Thereto the following assumptions were made: the log transformed hydraulic conductivity field is a second order stationary random space function, i.e. there is no trend in Y and the covariance between Y values at two different locations depends only on the separation distance between the locations. The axes of the spatial correlation are aligned with the horizontal and vertical directions and the spatial covariance is isotropic in the horizontal direction. Using an exponential covariance model to express the covariance C_{YY} in terms of the separation distance (ξ), the spatial covariance is given as

$$C_{YY}(\xi) = \sigma_Y^2 \cdot \exp\left(-\sqrt{\left(\frac{\xi_1}{\lambda_h}\right)^2 + \left(\frac{\xi_2}{\lambda_h}\right)^2 + \left(\frac{\xi_3}{\lambda_v}\right)^2}\right) \qquad (1)$$

where λ_h is the correlation length in longitudinal and in transverse horizontal direction and λ_v is the correlation length in transverse vertical direction. The mean hydraulic gradient and thus the mean flow vector are aligned in the horizontal direction with the principal axis of the spatial covariance function. There are no local sinks and sources so that the flow field is divergence free.

[11] The paper is organized in the following manner: In Section 2 we present the first- and second-order approximate solutions of the stochastic flow equation taken from literature. Subsequently, in section 3, we focus on the MC analyses including technical issues. Finally, in section 4, the statistics of the velocity from both MC analyses and the approximate solutions of the stochastic flow equation are compared and analyzed.

2. Approximate Solutions of Stochastic Flow Equation

[12] Below, approximations of the ensemble statistical parameters of the Darcy velocity based on first-order (superscript 1) and second-order (superscript 2) approximations of the perturbated continuity and Darcy equations in

conductivity fields of infinite extent are given. The following first- and second-order approximations of the mean (μ_{ql}), the variances (σ_q^2) and the spatial covariances ($C_q(\xi)$) of the Darcy velocity correspond to an exponential covariance model of the logarithm of the hydraulic conductivity (Y).

2.1. First-Order Approximate Solutions

[13] The mean Darcy velocity, ${}^{(1)}\mu_{ql}$, is given by *Dagan* [1989] by

$$\frac{{}^{(1)}\mu_{q_l}}{K_g J} = 1 + \frac{\sigma_Y^2}{6} \tag{2}$$

for $e = 1$, and

$$\frac{{}^{(1)}\mu_{q_l}}{K_g J} = 1 + \sigma_Y^2\left(\frac{1}{2} - \frac{1}{2}\frac{e^2}{1-e^2}\left(\frac{1}{e\sqrt{1-e^2}}\arctan\sqrt{\frac{1}{e^2}-1} - 1\right)\right) \tag{3}$$

for $e < 1$, where K_g is the geometric mean of the hydraulic conductivity and J is the mean hydraulic gradient.

[14] The variance of the longitudinal, ${}^{(1)}\sigma_{ql}^2$, the transverse horizontal, ${}^{(1)}\sigma_{qth}^2$, and the transverse vertical component, ${}^{(1)}\sigma_{qtv}^2$, of the velocity vector are given by *Dagan* [1989] for isotropic and by *Russo* [1995] for anisotropic cases by

$$\frac{{}^{(1)}\sigma_{q_l}^2}{\sigma_Y^2\left(K_g J\right)^2} = \frac{8}{15} \tag{4}$$

$$\frac{{}^{(1)}\sigma_{q_{th}}^2}{\sigma_Y^2\left(K_g J\right)^2} = \frac{{}^{(1)}\sigma_{q_{tv}}^2}{\sigma_Y^2\left(K_g J\right)^2} = \frac{1}{15} \tag{5}$$

for $e = 1$, and

$$\frac{{}^{(1)}\sigma_{q_l}^2}{\sigma_Y^2\left(K_g J\right)^2} = 1 + \frac{19e^3 - 10e^5}{16e(-1+e^2)^2} - \frac{e(13-4e^2)\arcsin\left[(1-e^2)^{\frac{1}{2}}\right]}{16(1-e^2)^{\frac{1}{2}}(-1+e^2)^2} \tag{6}$$

$$\frac{{}^{(1)}\sigma_{q_{th}}^2}{\sigma_Y^2\left(K_g J\right)^2} = \frac{e}{16(1-e^2)^{\frac{1}{2}}(-1+e^2)^2}\cdot\left(e\left(1-e^2\right)^{\frac{1}{2}} + 2e^3\left(1-e^2\right)^{\frac{1}{2}} + \arcsin\left[\left(1-e^2\right)^{\frac{1}{2}}\right] - 4e^2\arcsin\left[\left(1-e^2\right)^{\frac{1}{2}}\right]\right) \tag{7}$$

$$\frac{{}^{(1)}\sigma_{q_{tv}}^2}{\sigma_Y^2\left(K_g J\right)^2} = \frac{-3e^2}{4(-1+e^2)^2} + \frac{e(1+2e^2)\arcsin\left[(1-e^2)^{\frac{1}{2}}\right]}{4(-1+e^2)^{\frac{1}{2}}(-1+e^2)^2} \tag{8}$$

for $e < 1$.

[15] The covariance of the longitudinal, ${}^{(1)}C_{ql}(\xi_l')$, the transverse horizontal, ${}^{(1)}C_{qth}(\xi_l')$, and the transverse vertical component, ${}^{(1)}C_{qtv}(\xi'_l)$, of the velocity vector in longitudinal direction are given by *Russo* [1995] by

$$\frac{{}^{(1)}C_{q_l}\left(\xi_l'\right)}{\sigma_Y^2\left(K_g J\right)^2} = \int_{-1}^{+1}\left(\frac{1}{2} - \frac{r^2 e}{4[(1-r^2)+(r^2e^2)]^{\frac{3}{2}}}\cdot\left[4 - 5r^2 + r^4 + \left(3r^2 - r^4\right)e^2\right]\right)\cdot\left(1 - |r\xi_l'|\right)\exp\left(-|r\xi_l'|\right)dr \tag{9}$$

$$\frac{{}^{(1)}C_{q_{th}}\left(\xi_l'\right)}{\sigma_Y^2\left(K_g J\right)^2} = \int_{-1}^{+1}\frac{r^2 e(1-r^2)\left(1-|r\xi_l'|\right)}{4[(1-r^2)+r^2e^2]^{\frac{1}{2}}}\cdot\exp\left(-|r\xi_l'|\right)dr \tag{10}$$

$$\frac{{}^{(1)}C_{q_{tv}}\left(\xi_l'\right)}{\sigma_Y^2\left(K_g J\right)^2} = \int_{-1}^{+1}\frac{r^2 e(1-r^2)\left(1-|r\xi_l'|\right)}{4[(1-r^2)+r^2e^2]^{\frac{3}{2}}}\cdot\exp\left(-|r\xi_l'|\right)dr \tag{11}$$

for $e \le 1$ where $\xi'_l = \dfrac{\xi_l}{\lambda_h}$ is the normalized separation distance in longitudinal direction.

2.2. Second-Order Approximate Solutions

[16] The mean Darcy velocity, ${}^{(2)}\mu_{ql}$, is given by *Deng and Cushman* [1995] by

$$\frac{{}^{(2)}\mu_{q_l}}{K_g J} = \left(1 + \left(\frac{1}{2}+\beta\right)\sigma_Y^2 + \frac{1}{2}\left(\frac{1}{2}+\beta\right)^2\sigma_Y^4\right) \tag{12}$$

where $\beta = \dfrac{1}{2a^2}\left(1 - \dfrac{\arctan a}{e^2 a}\right)$ with $a = \sqrt{|1-e^2|/e^2}$ for $e < 1$ and $\beta = -\dfrac{1}{3}$ for $e = 1$.

[17] The variance of the longitudinal, ${}^{(2)}\sigma_{ql}^2$, the transverse horizontal, ${}^{(2)}\sigma_{qth}^2$, and the transverse vertical component, ${}^{(2)}\sigma_{qtv}^2$, of the velocity vector are given by *Deng and Cushman* [1995] by

$$\frac{{}^{(2)}\sigma_{q_l}^2}{\sigma_Y^2\left(K_g J\right)^2} = \frac{8}{15}\left(1 + \frac{7}{16}\sigma_Y^2\right) \tag{13}$$

for $e = 1$, and

$$\frac{{}^{(2)}\sigma_{q_l}^2}{\sigma_Y^2\left(K_g J\right)^2} = \frac{{}^{(1)}\sigma_{q_l}^2}{\sigma_Y^2\left(K_g J\right)^2} + \sigma_Y^2\left(\frac{3}{2} + \frac{3}{a^2}\left(1 - \frac{\arctan a}{e^2 a}\right) + \frac{3}{4a^4}\left(1 - \frac{\arctan a}{e^2 a}\right)^2 + \frac{6}{16a^2}\left(\frac{a^2+3}{a^2} + \frac{a^2-3}{e^2 a^3}\arctan a\right)\right) \tag{14}$$

for $e < 1$, and

$${}^{(2)}\sigma_{q_{th}}^2 = {}^{(1)}\sigma_{q_{th}}^2\left(1 + 2\sigma_Y^2\right) \tag{15}$$

$${}^{(2)}\sigma_{q_{tv}}^2 = {}^{(1)}\sigma_{q_{tv}}^2\left(1 + 2\sigma_Y^2\right) \tag{16}$$

for $e \le 1$, with $a = \sqrt{|1-e^2|/e^2}$.

[18] The above presented analytical expressions of *Deng and Cushman* [1995] are second order in σ_Y^2, however, without second-order head corrections. *Deng and Cushman* [1998] revisits the findings of *Deng and Cushman* [1995], considering second-order head corrections numerically. They found out that the second-order head corrections mainly influence the transverse components of the velocity. In detail, from Deng and Cushman's Figure 2 it can be deduced that the estimation of the variance of the transverse horizontal velocity component is not affected by second-

Table 2. Dimensions of the Modeling Domains, Grids, and Spatial Correlation Lengths of the Hydraulic Conductivity[a]

$e = \frac{\lambda_v}{\lambda_h}$	λ		Discretization		Size of the Domain	
	Hor., m	Ver., m	Hor., m	Ver., m	Hor., m	Ver., m
0.017	11.8	0.2	1	0.05	200	15
0.04	5	0.2	1	0.05	200	15
0.1	10	1	1	0.05	200	15
0.2	5	1	1	0.05	200	15
1	1	1	0.25	0.25	50	50

[a]The correlation lengths λ, λ_v, and λ_h correspond to an exponential correlation function; Hor. indicates horizontal, and Ver. indicates vertical.

order head corrections in an anisotropic case $e = 0.1$, but in the isotropic case $e = 1$. Furthermore Deng and Cushman's Figure 3 shows that the estimation of the variance of the transverse vertical velocity component is only slightly affected in the anisotropic case $e = 0.1$, but clearly in the isotropic case $e = 1$. Using second order in σ_Y^2 including second-order head corrections in the isotropic case as presented by *Deng and Cushman* [1998], the variance of both the transverse horizontal and transverse vertical velocity component are in between the here presented estimation based on equation (16) (second order without second-order head corrections) and the here presented estimation based on equation (7) (first order).

3. Monte Carlo Analyses

[19] In the following, the MC procedures including the generation of the hydraulic conductivity fields, numerical modeling of the velocity fields and the computation of ensemble parameters are described. Furthermore the reliability of the numerical results are discussed.

3.1. Layout and Computational Procedures

[20] The computational domain used for the MC analyses included 201 nodes in longitudinal, *l*, 201 nodes in transverse horizontal, *th*, and 301 nodes in transverse vertical direction, *tv*. The isotropic case departed from this scheme including only 201 nodes in the transverse vertical direction (Table 2). Realizations of the random space function, characterizing the spatial variability of the hydraulic conductivity, were generated with the Kraichnan generator using 65536 modes [*Kraichnan*, 1970]. The geometric mean of the hydraulic conductivity was 1.88×10^{-3} m/s for all conductivity fields. Five anisotropies (including one isotropic) and six different σ_Y^2 (ranging from 0.5 to 3.0 in 0.5 steps) were constructed. For each of these 30 cases, 10 fields were generated. The geostatistical input parameters for the Kraichnan generator are given in Table 2.

[21] The 3-D stationary flow equation, $\nabla(K_{\vec{x}}\nabla h_{\vec{x}}) = 0$ with $K_{\vec{x}}$ being the hydraulic conductivity and $h_{\vec{x}}$ being the head at position $\vec{x}$, was solved numerically, using the TRACE model [*Vereecken et al.*, 1994]. TRACE uses the standard Galerkin finite element method (FE) with hexagonal isoparametric elements. To solve the FE linear equations set, a conjugate gradient solver (CG) is used. The TRACE code is parallelized, and can be run on massive parallel computers [*Seidemann*, 1996; *Englert et al.*, 2004]. The computations were carried out on 32 processors of the "Juelich Multi Processor" (JUMP) supercomputer (IBM Regatta p690+ with 1312 Power4+ processors) at the Jülich research Center.

[22] No-flux Cauchy boundaries at the bottom, the top, the right and the left hand side of the domain were imposed. A constant head or Dirichlet condition was imposed at the front and the back of the domain resulting in a mean hydraulic gradient of 2.02×10^{-3} for all anisotropic cases and of 2.00×10^{-3} for the isotropic cases.

[23] The generation of the heterogeneous hydraulic conductivity field with the Kraichnan generator required between 2600 s and 2800 s. To solve the 3-D flow equation 1400 s to 2000 s of computation time was needed. About 8000 to 13000 CG iterations were needed to reach the convergence criterion of 1×10^{-8} m. The number of CG iterations and the computation time increased with increasing σ_Y^2.

3.2. Statistical Parameters

[24] Statistical parameters of a variable z at the position x_i were computed using the following formulas:

$$\mu_z = \frac{\sum_{i=1}^{n} z(x_i)}{n} \tag{17}$$

$$\sigma_z^2 = \frac{\sum_{i=1}^{n} (z(x_i) - \mu_z)^2}{n-1} \tag{18}$$

$$\gamma_z = \frac{n}{(n-1)(n-2)} \frac{\sum_{i=1}^{n} (z(x_i) - \mu_z)^3}{\sigma_z^3} \tag{19}$$

$$\eta_z = \frac{n(n+1)}{(n-1)(n-2)(n-3)} \frac{\sum_{i=1}^{n} (z(x_i) - \mu_z)^4}{\sigma_z^4} - \frac{3(n-1)^2}{(n-2)(n-3)} \tag{20}$$

$$C_z(\xi) = \frac{1}{m} \sum_{i=1}^{m} (z(x_i) \cdot z(x_i + \xi)) - \mu(z(x_i)) \cdot \mu(z(x_i + \xi)) \tag{21}$$

$$\rho_z(\xi) = \frac{C_z(\xi)}{\sigma(z(x_i)) \cdot \sigma(z(x_i + \xi))} \tag{22}$$

where n is the number of observations, m is the number of paired observations, μ is the arithmetic mean, σ^2 is the variance, γ is the skewness, η is the kurtosis, $C(\xi)$ the spatial covariance and $\rho(\xi)$ the spatial correlation of the variable z for the separation vector ξ.

[25] Nonparametric estimates of a representative value and of the spreading of the distribution were estimated from the median and the squared absolute value of half the difference between the 15.87 percentile and the 84.13 percentile. For a normal distribution, these quantile based estimates correspond with μ and σ^2. For nonparametrical estimation of spatial correlations an indicator approach was used, based on the following transform:

$$ind(x_i) = \begin{cases} 1 & \text{if } z(x_i) \le cut \\ 0 & \text{otherwise} \end{cases} \tag{23}$$

where ind_i is the transformed value of $z(x_i)$ for a given cutoff value *cut*.

[26] In the scope of the MC analysis statistical parameters were derived for single realizations and for all realizations of a certain case, where the parameters are based on the values of, in our case, ten realizations. The latter one are called ensemble parameters. To quantify the statistical convergence of a particular ensemble parameter at a 95% confidence interval the "jackknife method" [*Wonnacott and Wonnacott*, 1985] was used. Statistical computations were carried out using GSLIB [*Deutsch and Journel*, 1998] and SAS 8.2 (SAS Institute Inc., North Carolina) software.

3.3. Generated Hydraulic Conductivity Fields

[27] To illustrate the reliability of the stochastically generated heterogeneous K fields, the case with the input parameters $Y = -6.277$ ln(m/s), $\sigma_Y^2 = 3$, $\lambda_h = 11.8$ m and $\lambda_v = 0.2$ m was analyzed in detail.

[28] The ensemble mean of the generated Y fields was $Y = -6.283$ ln(m/s), which corresponds to a deviation from the preset mean of 0.10%. Within the ten realizations the maximum mean was $Y = -6.295$ ln(m/s), the minimum mean was $Y = -6.360$ ln(m/s), which corresponds to a maximum deviation from the preset mean of 1.32%. The ensemble σ_Y^2 was 3.009, which corresponds to a deviation from the preset σ_Y^2 of 0.30%. The maximum σ_Y^2 was 3.008, the minimum σ_Y^2 was 2.943 which corresponds to a maximum deviation from the preset variance of 0.26%.

[29] It could be observed that there was a very good accordance between the generated Y field and the a priori prescribed covariances for the horizontal directions (Figures 1a and 1b). In the vertical direction (Figure 1c), a very good fit between the ensemble covariance of the generated Y fields and the a priori prescribed covariances was found up to a lag distance of about ten meters. At higher lag distances the ensemble correlations began to oscillate but with a very small amplitude.

[30] The presented case was the most critical one amongst all the 30 cases of this study. The other 29 cases showed even smaller deviations from the prescribed parameters.

3.4. Convergence and Accuracy of Flow Simulation

[31] To control the numerical convergence of the flow simulations we analyzed the convergence behavior of the velocity statistics of three selected single realizations: $e = 0.017$ at $\sigma_Y^2 = 1$, $e = 0.017$ at $\sigma_Y^2 = 3$ and $e = 1$ at $\sigma_Y^2 = 3$. For these realizations we successively decreased the convergence criteria within the CG until the statistical parameters of the velocity converged. This occurred at a CG convergence criteria of 1×10^{-8} m. Flow simulations using a more stringent convergence criteria for the CG of 1×10^{-14} m led to identical velocity statistics within at least three significant digits.

[32] To measure the accuracy of the flow simulations the relative mass balance error was considered first for the entire domain and second for every element in the domain. The mass balance, defined as (inflow − outflow)/(total volume), was calculated for all cases and all realizations. The relative mass balance error for the entire domain increased with increasing σ_Y^2, but was not influenced by the anisotropy ratio *e*. The mean relative mass balance error for the entire domain was 9×10^{-5}% at $\sigma_Y^2 = 0.5$ and was 5×10^{-4}% at $\sigma_Y^2 = 3$. Within the 300 realizations the maximum of the relative mass balance error for the entire domain was 4×10^{-4}% and 3×10^{-3}% for $\sigma_Y^2 = 0.5$ and $\sigma_Y^2 = 3$ respectively.

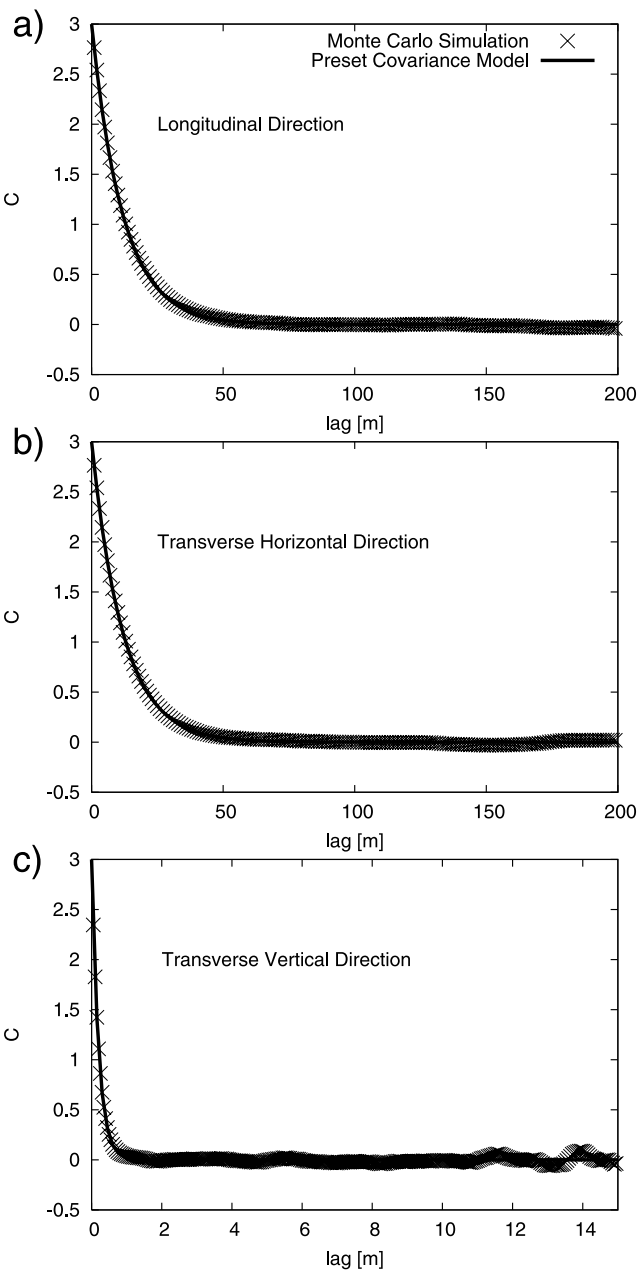

Figure 1. Preset covariance function of Y and ensemble covariances from generated Y fields using the Kraichnan generator shown for the three directions of the modeling domain in the case $e = 0.017$ and $\sigma^2 = 3.0$.

[33] On the basis of velocity data at the nodes of lateral surfaces of an element, the mean velocities normal to the surfaces of single elements were calculated. We then standardized the mean velocities by the corresponding area of an element surface and we calculated the resulting velocities into or out of an element. Subsequently the local mass balances were calculated for every single element by multiplying the afore mentioned velocities times the time step (0.1 d) used in the global mass balance computation. Evaluating only the inner core of the domain (see section 3.5) the mean relative mass balance error for single elements was

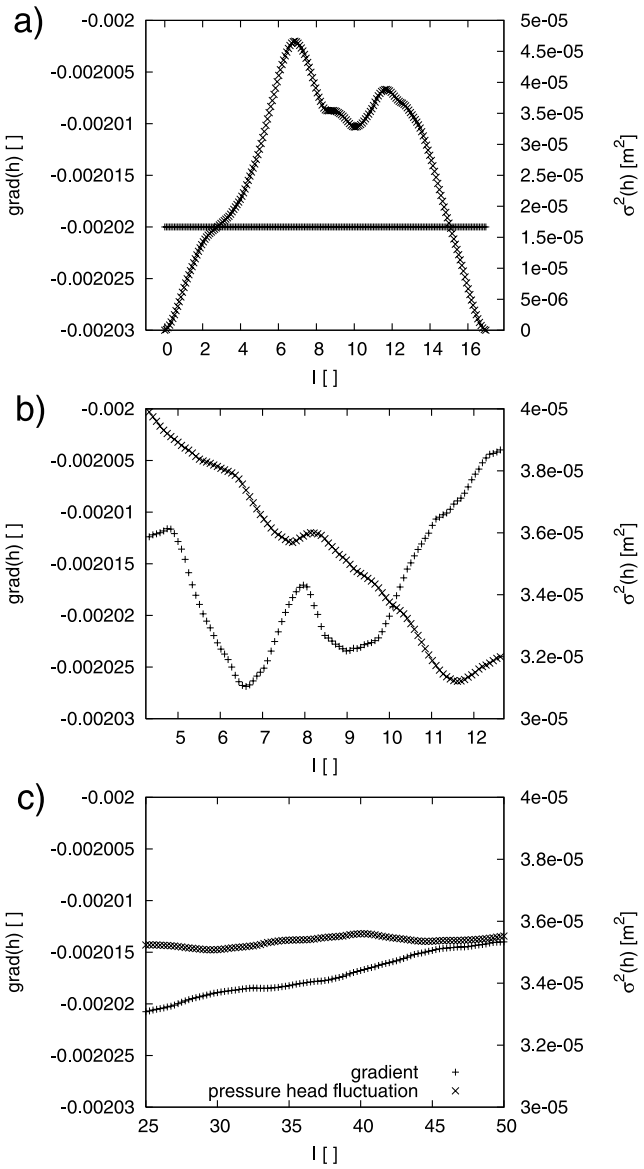

Figure 2. Ensemble mean gradient and ensemble pressure head fluctuations in nodal surfaces as a function of the position in the domain, based on a heterogeneous K field with $e = 0.017$ and $\sigma_Y^2 = 1$: (a) in the longitudinal direction, (b) in the transverse horizontal direction, and (c) in the transverse vertical direction. The abscissae represent the normalized position I; in Figures 2a and 2b, $I = x/\lambda_h$, and in Figure 2c, $I = x/\lambda_v$.

1.9×10^{-4}% at $\sigma_Y^2 = 0.5$ and was 7.7×10^{-4}% at $\sigma_Y^2 = 3$. The maximum relative mass balance error was 5.4×10^{-3}% and 1.8×10^{-1}% for $\sigma_Y^2 = 0.5$ and $\sigma_Y^2 = 3$ respectively. These values were assumed to be small enough to avoid a significant impact on the velocity statistics.

3.5. Mean Gradient, Head Fluctuations, and Boundary Effects

[34] It is well known that boundary conditions, no flow boundaries as well as constant head boundaries, have a detectable impact on the statistics of the pressure head as well as of the Darcy velocity in the vicinity of the boundaries. In this context *Rubin and Dagan* [1988] and *Rubin and Dagan* [1989] showed the influence of boundary conditions on head variabilities in a flow domain using a first order in σ_Y^2 analytical solution of the stochastic flow equation for 2-D isotropic cases. *Bellin et al.* [1992], *Oliver and Christakos* [1996], *Salandin and Fiorotto* [1998], and *Hassan et al.* [1998], for example, observed boundary effects on head and flux variabilities using MC analyses for 2-D cases.

[35] *Naff et al.* [1998a] shows boundary effects in the numerically simulated velocity fields in detail for 3-D anisotropic hydraulic conductivity fields. They demonstrated that the statistics of the longitudinal component of the velocity are not visibly influenced by boundary conditions nor in longitudinal neither in transverse transects. The variances of both transverse components of the velocity are affected in longitudinal direction, converging toward zero at the constant head boundaries. The variance of the transverse horizontal component is affected in transverse horizontal direction, converging toward zero at the no flux boundaries. It is not affected in transverse vertical direction. The variance of the transverse vertical component is affected in transverse vertical direction, converging toward zero at the no flux boundaries. It is not affected in transverse horizontal direction.

[36] In our study the influence of the boundary conditions on head, mean gradient and velocity statistics were analyzed as follows: In a first step the statistics of the head and of the velocity components were calculated in each realization for every nodal surface parallel to a lateral boundary. In a second step ensemble mean and variance in a surface at a certain distance from the boundary were calculated from the velocity statistics of the single realizations. The ensemble gradients and head fluctuations are directly calculated based on the values of all realizations within a certain case. The computed ensemble parameters of each slice were based on at least 100000 single values. In the following the focus is first on boundary effects on head fluctuations and mean gradients and second on velocity statistics.

[37] The ensemble mean gradient of the entire domain was computed by subtracting the ensemble mean pressure head at the front plane from the ensemble mean pressure head at the back plane of the domain and dividing the difference by the length of the entire domain. Therefore the mean gradient of the entire domain is predefined by the models' extend and constant head boundary conditions at the front and the back of the domain. These data were used to set up an equation describing the mean pressure head as a linear function of the position along the mean flow direction (q_l direction). Consequently the head fluctuations for every plane parallel to the front and back planes of the domain are the mean squared residuals of the individual head values within a plane related to the corresponding pressure head value defined by the linear function. For the case $e = 0.017$ and $\sigma_Y^2 = 1$ ensemble mean gradients for the entire domain and the corresponding head fluctuations are shown in Figure 2a. It shows, as expected, that the head fluctuations are strongly influenced by the constant head boundaries converging to zero at these boundaries.

[38] Evaluating only the inner core of the domain (see last paragraph of this section) mean gradient and head fluctuations were computed slicewise and parallel to the mean flow

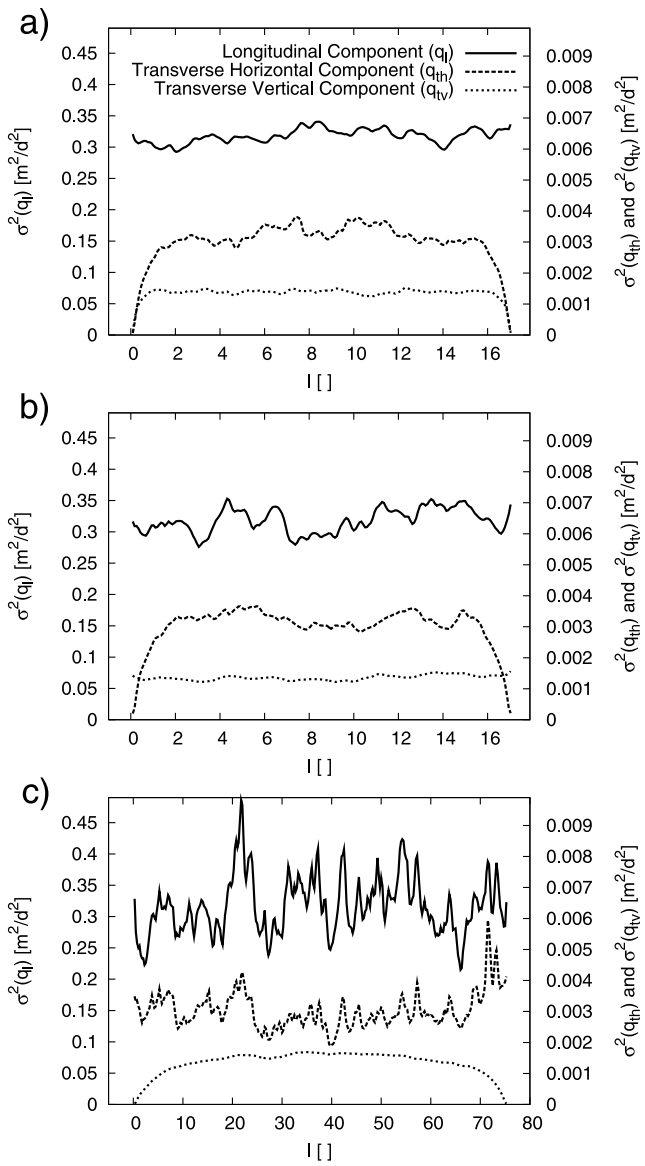

Figure 3. Ensemble variances of the Darcy velocity vector components in nodal surfaces as a function of the position in the domain, based on a heterogeneous K field with $e = 0.017$ and $\sigma_Y^2 = 1$: (a) in the longitudinal direction, (b) in the transverse horizontal direction, and (c) in the transverse vertical direction. The abscissae represent the normalized position I; in Figures 3a and 3b, $I = x/\lambda_h$, and in Figure 3c, $I = x/\lambda_v$.

direction. Mean pressure heads were computed at the front line and the back line of each slice. For each slice these mean pressure head values and the distance between front and back of the inner core were subsequently used to set up an equation describing the mean pressure head as a linear function of the position along the q_l direction. Consequently the mean gradients are equal to the slopes of these equations and the head fluctuations are represent by the mean squared residuals of the individual head values related to the corresponding value defined by the linear equations. Figures 2b and 2c display the resulting ensemble gradients and ensemble head fluctuations as a function of the position in *th* direction and *tv* direction, respectively. Figures 2b and 2c show that the ensemble gradient and the ensemble head fluctuations are still varying with the position in *th* direction as well as in *tv* direction. This is more pronounced in *th* direction than in *tv* direction, which is due to the much smaller number of integral scales of Y in the horizontal direction. The ensemble mean gradient for the inner core (not shown) shows only 0.1% deviation from the ensemble mean gradient of the entire domain.

[39] The previous shown analyses of ensemble gradients and ensemble head fluctuations was performed for $e = 1$ and $e = 0.017$, including $\sigma_Y^2 = 1.0$ and $\sigma_Y^2 = 3.0$. An integrated analysis of the results shows that with increasing σ_Y^2 and decreasing e, the head fluctuations increase from $1{,}78 \times 10^{-6}$ m^2 at $e = 1$ and $\sigma_Y^2 = 1$ to 1.11×10^{-4} m^2 at $e = 0.017$ and $\sigma_Y^2 = 3$. Differences between the preset mean gradient and the ensemble mean gradient of the inner core are higher for the isotropic than for the strongly anisotropic case with a maximum deviation of 2.25% at $e = 1$ and $\sigma_Y^2 = 3$.

[40] In Figure 3 the variances of the velocity components in nodal surfaces are presented for the different directions as a function of the normalized position relative to the point of origin of the velocity field for the case $\sigma_Y^2 = 1$ and e = 0.017. Figure 3a shows that in the longitudinal direction with constant head boundaries the variances of the transverse components are affected up to 2 λ_h and converge toward 0 at the edges. The variance of the longitudinal component is not visibly affected. From Figures 3b and 3c, it can be observed that in the transverse directions with impervious boundaries the variance of the longitudinal component of the velocity is unaffected. Contrary the horizontal transverse component is affected in horizontal transverse direction, *th* direction, up to 2 λ_h and the vertical transverse component is affected in vertical transverse direction, *tv* direction, up to 10 λ_v. Both converge toward 0 at the edges.

[41] The previous analysis was performed for each case in the MC analyses, and the impact of variations in σ_Y^2 and e on boundary effects was studied. In general, there were only negligible boundary effects on $\sigma^2(q_l)$ in *th* and *tv* direction, on $\sigma^2(q_{tv})$ in *th* direction, and on $\sigma^2(q_{th})$ in *tv* direction. The most pronounced impact of boundary conditions was on

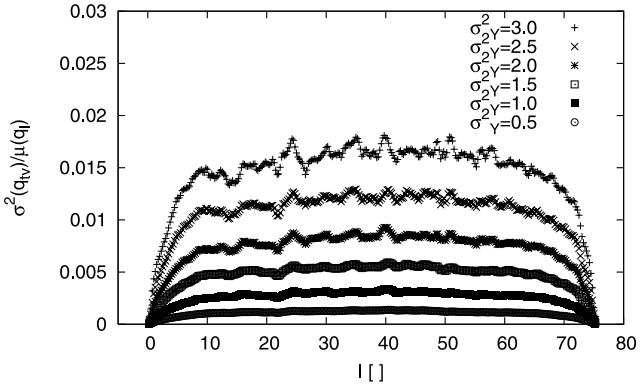

Figure 4. Effect of the variance of the logarithm of the hydraulic conductivity, σ_Y^2, on the estimated normalized variances of the vertical transverse component of the Darcy velocity in horizontal nodal surfaces parallel to the mean flow direction as a function of the distance from the bottom boundary. The abscissa represents the normalized position $I = x/\lambda_v$. The anisotropy of the K fields is $e = 0.017$.

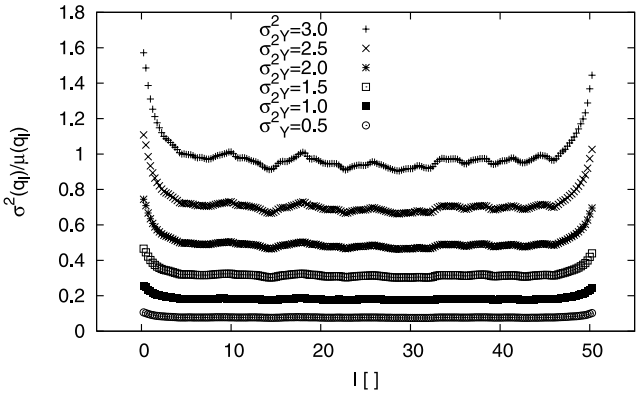

Figure 5. Effect of the variance of the logarithm of the hydraulic conductivity, σ_Y^2, on the estimated normalized variances of the longitudinal component of the Darcy velocity in vertical nodal surfaces parallel to the mean flow direction as a function of the distance from the front boundary. The abscissa represents the normalized position $I = x/\lambda_h$. The K fields are isotropic, $e = 1$.

$\sigma^2(q_{tv})$ in *tv* direction (Figure 4). The range of influence of the no-flux boundaries increases with increasing σ_Y^2 and with increasing anisotropy (decreasing *e*). The influence in range increases from 2 λ_v at $e = 1$ and $\sigma_Y^2 = 0.5$ to 15 λ_v at e = 0.017 and $\sigma_Y^2 = 3.0$. The effect of no-flux boundaries on $\sigma^2(q_{th})$ in *th* direction increases with increasing σ_Y^2 and decreases with increasing anisotropy. The influence range is 0.5 λ_h at $e = 0.017$ and $\sigma_Y^2 = 0.5$ and 4 λ_h at $e = 1$ and $\sigma_Y^2 = 3$. The constant head boundaries, edges in *l* direction, influence the variances of all components of the Darcy velocity vector. Both $\sigma^2(q_{th})$ and $\sigma^2(q_{tv})$ are converging to 0 within 2 λ_h in *l* direction. This behavior is not affected by variations in σ_Y^2 and *e*. Contrary at higher σ_Y^2 (not visible at the relative small σ_Y^2 of Figure 3a) $\sigma^2(q_l)$ increases toward the edge (Figure 5). This effect increases with increasing σ_Y^2 and decreases with increasing anisotropy. For $e = 0.017$ and $\sigma_Y^2 = 0.5$ the influence of the constant head boundary on $\sigma^2(q_l)$ is negligible, whereas the range of influence increases to 4 λ_h for $e = 1$ and $\sigma_Y^2 = 3$ (Figure 5).

[42] To exclude the boundary effects, only velocities within an inner core of the entire flow domains were considered. This inner core was 100 m in *l* direction, 100 m in *th* direction and 5 m in *tv* direction for all the anisotropic cases and it was 37.5 m in all directions for the isotropic cases. For all the cases with $e = 0.017$, $e = 0.04$ and $e = 1$ this ensures negligible boundary effects on the inner core. For the cases with $e = 0.1$ and $e = 0.2$ the exclusion of boundary effects is ensured up to $\sigma_Y^2 = 1.0$ for all components of the velocity. For higher σ_Y^2 the *tv* component is somewhat underestimated. Contrary the influence of boundaries on the *l* and *th* components of the velocity are again negligible within the inner core.

4. Results

[43] After excluding the boundary effects, the Monte Carlo analyses allow for a detailed statistical characterization of the velocity as a function of the variance and the correlation lengths in horizontal and vertical direction of the logarithm of the hydraulic conductivity, Y. Within the reliability discussed in Section Monte Carlo Analyses, this permits a comparison with first- and second-order approximate solutions of the stochastic flow equation. In the following the results are discussed, first with a focus on univariate velocity statistics and second on spatial velocity statistics.

4.1. Univariate Velocity Statistics

[44] The MC analyses showed that with increasing σ_Y^2 and increasing anisotropy the probability density function of q_l exhibited an increasing asymmetry with a tail to the right. This was expressed by an increase in skewness from 1.3 at $e = 1$ and $\sigma_Y^2 = 0.5$ toward a value of 9.9 at $e = 0.017$ and $\sigma_Y^2 = 3.0$ (see Figure 6). Simultaneously the kurtosis increased from 3.1 toward a value of 188 (see Figure 7a). Excluding occasionally negative q_l values, the accordant values for the skewness and kurtosis of log-transformed values of q_l ranged between -0.2 and -0.03. This suggests that the q_l distribution is better described by a log normal than a normal distribution. However, this could not be confirmed with the Kolmogorov Smirnov test for normality. In this context it is important to consider that with increasing σ_Y^2 and decreasing anisotropy the probability of negative values for the longitudinal velocity component increases. For $\sigma_Y^2 < 1.5$ the probability for negative q_l values was undetectable small. For $\sigma_Y^2 = 3$, the probability increased to 0.00002% at $e = 0.017$ and to 0.008% in the isotropic case. Negative q_l values are well known from other 2-D and 3-D MC analyses on flow in heterogeneous media including $\sigma_Y^2 > 1.5$ [e.g., *Tompson and Gelhar*, 1990; *Salandin and Fiorotto*, 1998; *Janković et al.*, 2003a]. They can occur in cases where a relatively high conductive flow path is surrounded by relatively low hydraulic conductivities and the shape of the conductive flow path includes sections in reverse direction with respect to the mean flow direction.

[45] The probability density functions of both transverse components showed an increase of the kurtosis with increasing σ_Y^2 (see Figures 7b and 7c). In the isotropic case (e = 1), the kurtosis of the transverse components were quite similar to those of the longitudinal component. In the anisotropic

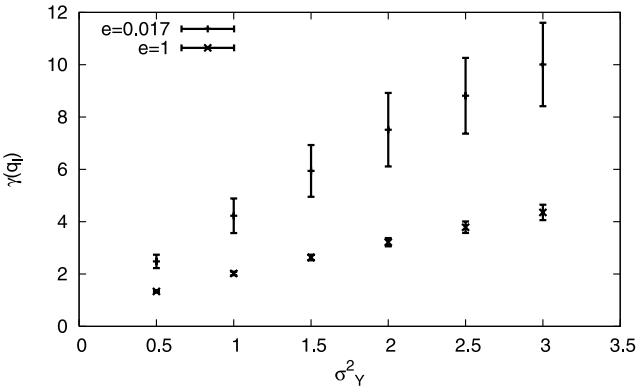

Figure 6. Estimated ensemble skewness, γ, of the longitudinal component of the velocity vector, q_l, as a function of the variance of the logarithm of the hydraulic conductivity, σ_Y^2, for an isotropic ($e = 1$) and a strongly anisotropic ($e = 0.017$) case. The error bars denote the convergence of the skewness with regard to a 95% confidence interval.

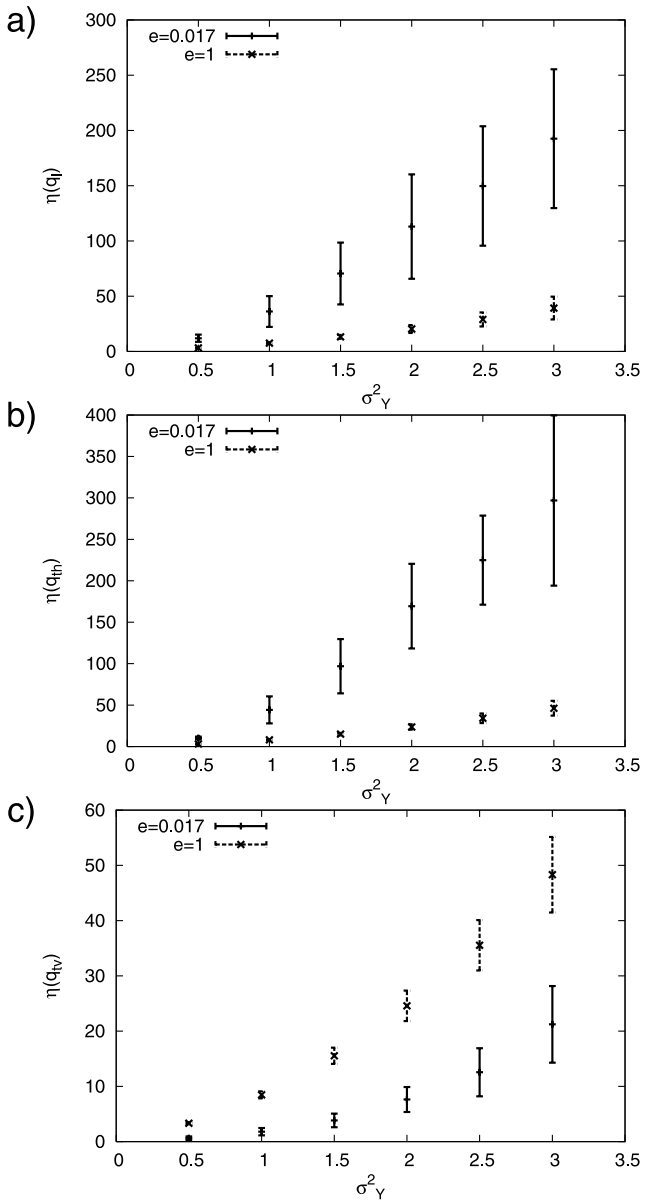

Figure 7. Estimated ensemble kurtosis, η, of the velocity vector as a function of the variance of the logarithm of the hydraulic conductivity, $\sigma_Y{}^2$, for an isotropic (e = 1) and a strongly anisotropic (e = 0.017) case: (a) longitudinal component, (b) transverse horizontal component, and (c) transverse vertical component. The error bars denote the convergence of the kurtosis with regard to a 95% confidence interval.

case (e = 0.017) an increase of σ_Y^2 from 0.5 to 3.0 caused the ensemble kurtosis of q_{th} to increase from 10 to 296 and the kurtosis of q_{tv} to increase from 0.6 to 21. It is important to note that in Figure 7b the ensemble kurtosis of the anisotropic case is based on only 9 realizations. The excluded realization shows a factor 5 higher kurtosis than the ensemble kurtosis of the other 9 realizations and therefore would distort the general pattern of the ensemble kurtosis. It is remarkable that this special realization cannot be identified as an outlier concerning mass balance errors or other statistical parameters.

[46] Figure 8 shows the mean of q_l and the variances of q_l, q_{th} and q_{tv} as function of σ_Y^2 for both, an isotropic and a strongly anisotropic case. Figures 8a and 8e show that $\mu(q_l)$ increases stronger with increasing σ_Y^2 in the anisotropic case than in the isotropic case. It can be concluded that the estimation of $\mu(q_l)$ by second-order approximation fitted quite well to the MC results, for both, the isotropic and the anisotropic cases. The median value of q_l shows no visible response to variations in σ_Y^2 as well as in e (see Figures 8a and 8e).

[47] For the isotropic cases up to $\sigma_Y^2 = 0.5$ (Figures 8b, 8c, and 8d) it can be concluded that $\sigma^2(q_l)$, $\sigma^2(q_{th})$ and $\sigma^2(q_{tv})$ derived from the MC analysis agree better with first-order than second-order approximation. This is astonishing because one would expect the second-order approximation to fit better to the estimates from the MC analyses. However, the second-order approximations in section 2.2 do not consider second order head corrections, which is likely the reason for the discrepancies between second-order estimations and the results of the MC analyses at $0.5 < \sigma_Y^2 \leq 1.5$. On the other hand with decreasing σ_Y^2 first- and second-order approximations converge. Therefore at $\sigma_Y^2 = 0.01$ and $e = 1$ there are only little differences between first-order ($\sigma^2(q_{th}) = \sigma^2(q_{tv}) = 7.0 \times 10^{-5}$ m^2/d^2) and second-order ($\sigma^2(q_{th}) = \sigma^2(q_{tv}) = 7.2 \times 10^{-5}$ m^2/d^2) estimation. Also a MC analyses at $\sigma_Y^2 = 0.01$ and $e = 1$ showed a similar result ($\sigma^2(q_{th}) = \sigma^2(q_{tv}) = 5.4 \times 10^{-5}$ m^2/d^2), slightly below first- and second-order estimation. Note that the MC analyses with $e = 1$ and $\sigma_Y^2 = 0.01$ was not discussed in further details but is based on the same procedures presented for those MC analyses including $e = 1$.

[48] For the isotropic cases the second-order approximation of $\sigma^2(q_l)$ is in accordance with the MC analyses for $0.5 < \sigma_Y^2 \leq 1.5$. A further increase of σ_Y^2 results in higher values of $\sigma^2(q_l)$ than predicted by second-order approximation. With increasing σ_Y^2, $\sigma^2(q_{th})$ and $\sigma^2(q_{tv})$ derived from the MC analysis fit better with the second-order approximation than with first-order approximation. It is interesting to note that the non parametric estimates of the spreading of the velocity distributions correspond well with the first-order approximation of $\sigma^2(q_l)$, $\sigma^2(q_{th})$ and $\sigma^2(q_{tv})$.

[49] In the anisotropic cases an agreement between the results of the MC analysis and the second-order approximation can be observed for $\sigma^2(q_{tv})$ as a function σ_Y^2 (Figure 8h). The non parametric estimates of $\sigma^2(q_{tv})$ are slightly below these results. For $\sigma_Y^2 < 1$, $\sigma^2(q_l)$ obtained from second-order approximation and from MC analyses are in good agreement (Figure 8f). For $\sigma_Y^2 \geq 1$ the second-order approximations of $\sigma^2(q_l)$ underestimate the MC results. In addition $\sigma^2(q_l)$, estimated from MC analyses, increases more rapidly with σ_Y^2 than the second-order approximations. First-order approximations of $\sigma^2(q_l)$ underestimate both second-order approximations and MC results of $\sigma^2(q_l)$, also for small σ_Y^2. Non parametric estimates of $\sigma^2(q_l)$ agree with the first-order approximation at $\sigma_Y^2 = 0.5$. For higher σ_Y^2, non parametric estimates of $\sigma^2(q_l)$ are in between first- and second-order approximations, converging toward the second-order approximation. The largest discrepancies between the approximate solutions of the stochastic flow equation and the MC analyses are observed for $\sigma^2(q_{th})$, increasing more rapidly with increasing σ_Y^2 in the MC analyses (Figure 8g). Non parametric estimates of $\sigma^2(q_{th})$ are slightly higher than second-order approximations.

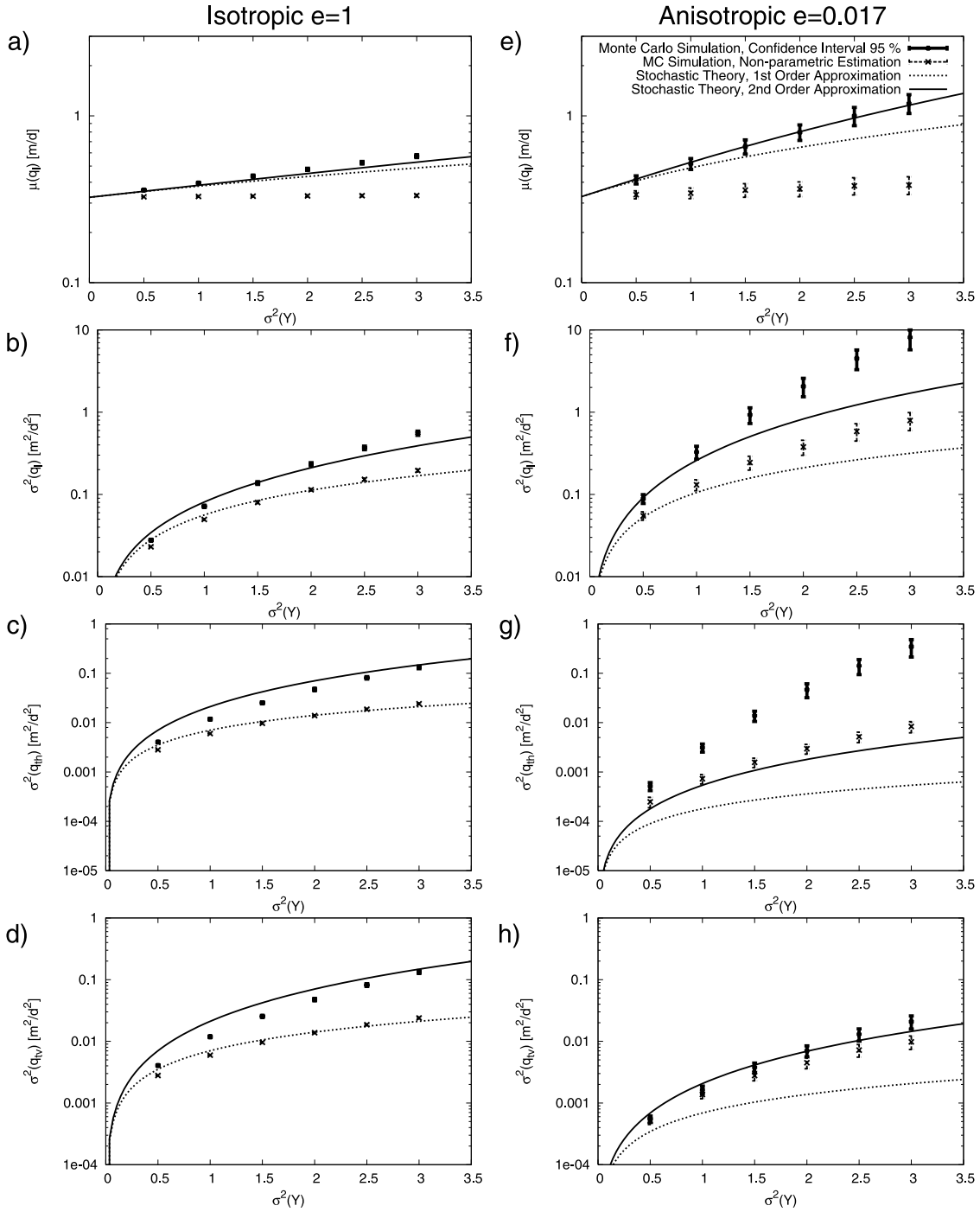

Figure 8. Estimated univariate ensemble statistics of the components of the Darcy velocity vector, $\vec{q}$, as a function of the variance of the logarithm of the hydraulic conductivity, σ_Y^2: (a and e) mean Darcy velocity, $\mu(q_l)$, (b and f) variance of the longitudinal component, $\sigma^2(q_l)$, (c and g) variance of the transverse horizontal component, $\sigma^2(q_{th})$, and (d and h) variance of the transverse vertical component, $\sigma^2(q_{tv})$, for an isotropic and a strongly anisotropic K field. In some cases the confidence interval of a parameter is so small that the error bars are not visible.

[50] Figure 9 gives an insight into the variances of the velocity components as a function of the anisotropy ratio, e, for $\sigma_Y^2 = 0.5$ and $\sigma_Y^2 = 3$. For small σ_Y^2, $\sigma^2(q_l)$ decreases slightly with increasing e (Figure 9a). The $\sigma^2(q_l)$ obtained from MC analyses is in good agreement with the second-order approximation. The non parametric estimates of $\sigma^2(q_l)$ agree well with the first-order approximation. For $\sigma_Y^2 = 3$, $\sigma^2(q_l)$ from the MC analyses show a stronger increase with decreasing e than predicted by second-order approximation (Figure 9d). The non parametric estimates of $\sigma^2(q_l)$ from MC analyses fall in between first- and second-order approximation.

[51] For small σ_Y^2, both stochastic approximations and the MC analyses predict increasing values of $\sigma^2(q_{th})$ with increasing e. The second-order approximation is in better

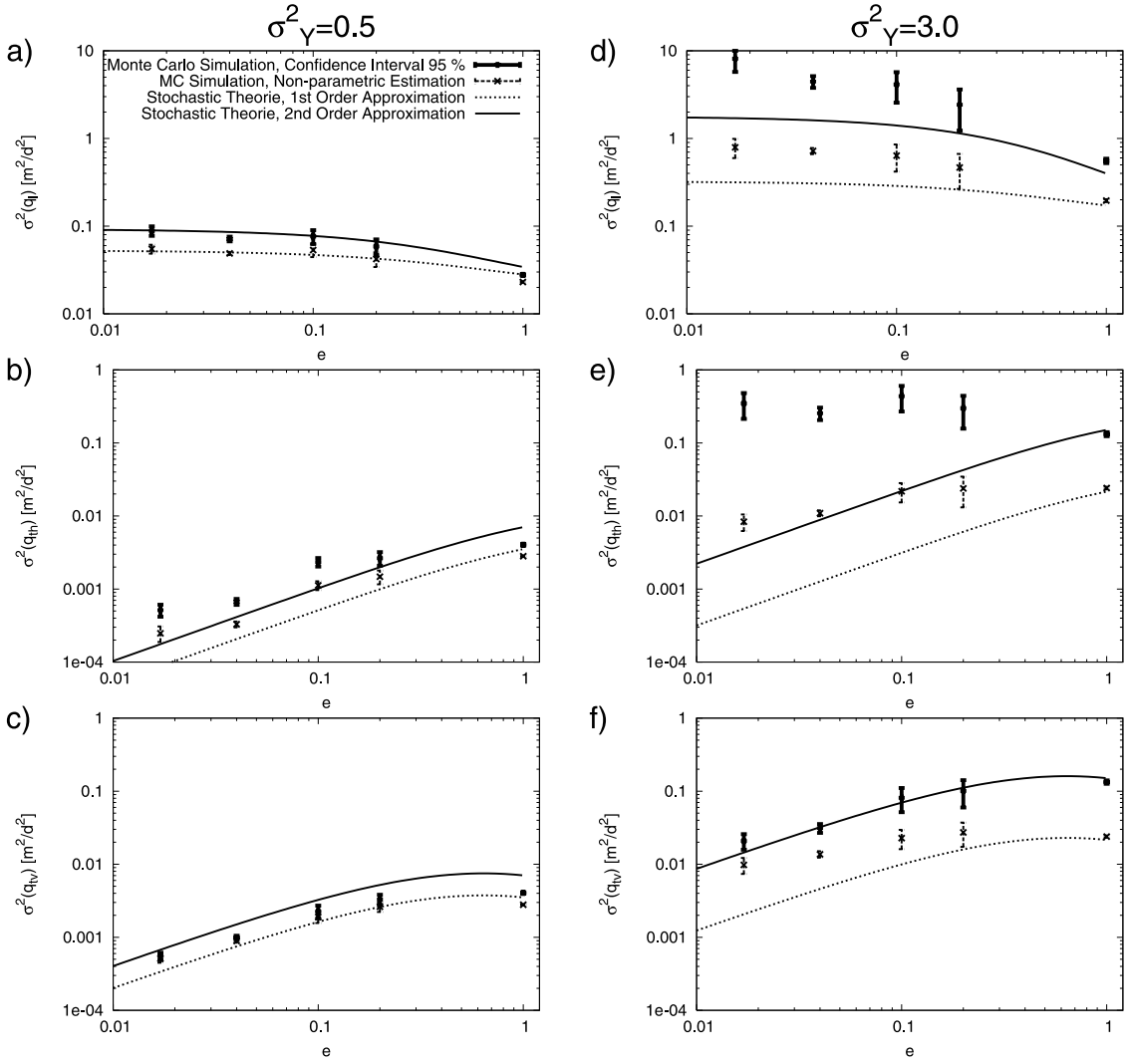

Figure 9. Estimated ensemble variances of the components of the Darcy velocity vector, $\vec{q}$, as a function of the anisotropy, e: (a and d) variance of the longitudinal component, $\sigma^2(q_l)$, (b and e) variance of the transverse horizontal component, $\sigma^2(q_{th})$, and (c and f) variance of the vertical transverse component, $\sigma^2(q_{tv})$, for two different variances of the logarithm of the hydraulic conductivity, ${\sigma_Y}^2$. In some cases the confidence interval of a parameter is so small that the error bars are not visible.

agreement with the MC analyses than the first-order approximation (Figure 9b). This agreement is not found for the cases $\sigma_Y^2 = 3$ (Figure 9e). While the first- and second-order approximate solutions of the stochastic flow equation predicted an increasing value of $\sigma^2(q_{th})$ with increasing e, the MC analyses predict relatively constant and larger values of $\sigma^2(q_{th})$. It is remarkable that the $\sigma^2(q_{th})$ derived from MC analyses is of the same order of magnitude as the second-order approximation of $\sigma^2(q_{th})$ for high values of e, which converges to 0.3 (not shown in Figure 9e). The non parametric estimated $\sigma^2(q_{th})$ also shows a relatively constant value but at a lower level.

[52] Both first- and second-order approximations and the MC analyses show increasing $\sigma^2(q_{tv})$ values with increasing e. At $\sigma_Y^2 = 0.5$, $\sigma^2(q_{tv})$ derived from MC analyses fits better to the second-order approximation at small e, and better to the first-order approximation when e is closer to 1 (Figure 9c). At $\sigma_Y^2 = 3.0$, $\sigma^2(q_{tv})$ derived from MC analyses fits well to the second-order approximation (Figure 9f). The non parametric estimation of $\sigma^2(q_{tv})$ fits better to second-order approximation at small e and better to first-order approximation at e close to 1 at $\sigma_Y^2 = 0.5$ and $\sigma_Y^2 = 3.0$.

4.2. Spatial Correlation of Velocity

[53] The MC analyses shows that with increasing σ_Y^2 the spatial correlation decreases more rapidly with separation distance (see Figure 10). This can be observed for longitudinal as well as for the transverse components and is more pronounced for the anisotropic than for the isotropic case. For the correlation of the transverse velocity components simultaneously the negative correlations, in absolute terms, decrease with increasing σ_Y^2. In contrast to this, the first-order approximation of the spatial correlations of q are independent of σ_Y^2. However, in the isotropic case (Figures 10a, 10b, and 10c) the agreement between the MC analyses and the first-order approximation is fairly good, at least for $\sigma_Y^2 \leq 1$. Also in the anisotropic case, the longitudinal component ρ (q_l) is in good agreement with the first-order

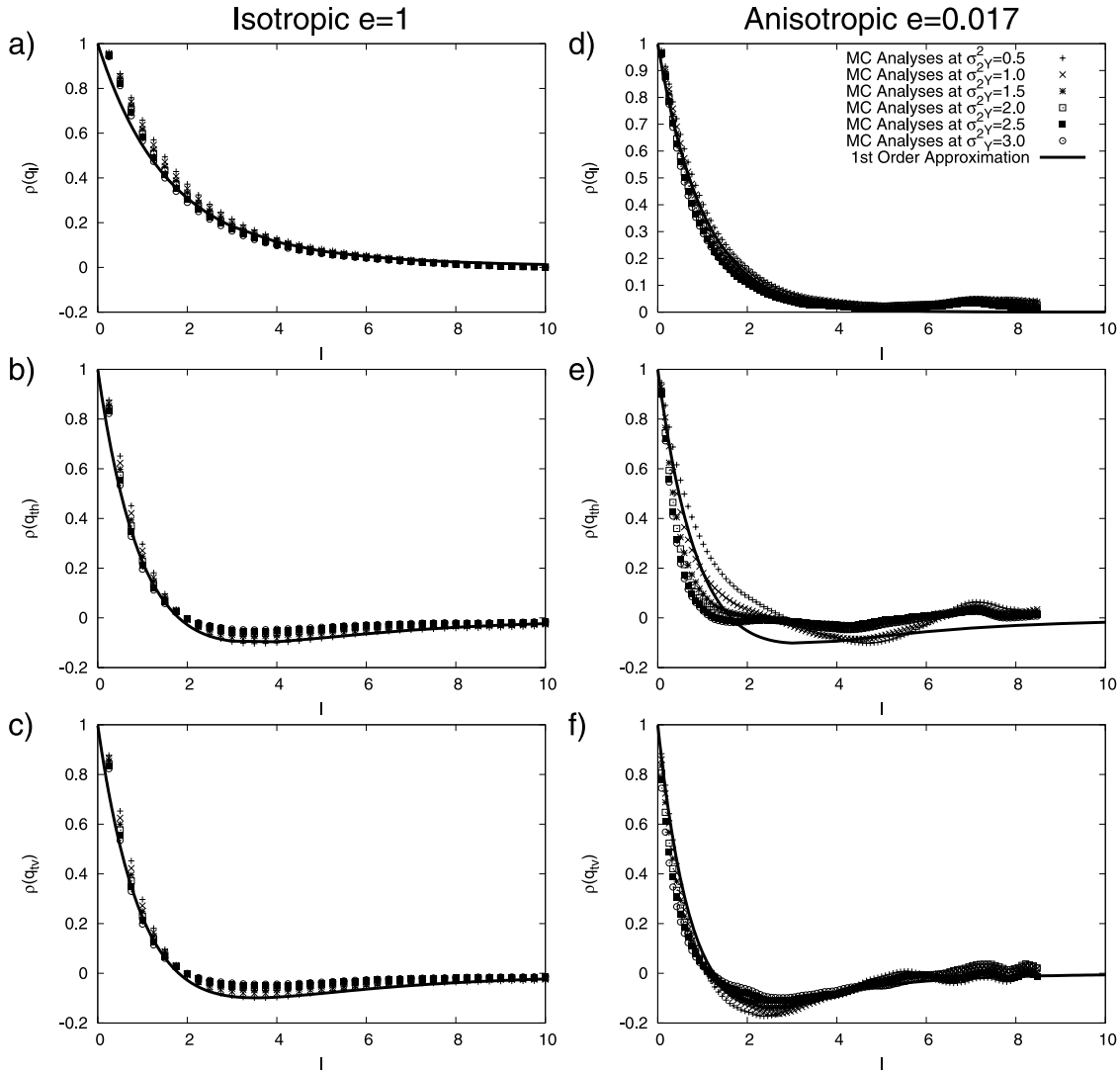

Figure 10. Estimated correlations in the longitudinal direction for different variances of the logarithm of the hydraulic conductivity, $\sigma_Y{}^2$. Along the abscissa the normalized lag distance, $I = \xi/\lambda_h$, is applied. The correlation is given for the three components of the velocity vector: (a and d) longitudinal component, $\rho(q_l)$, (b and e) horizontal transverse component, $\rho(q_{th})$, and (c and f) vertical transverse component, $\rho(q_{tv})$.

approximation up to $\sigma_Y^2 = 3$ (see Figure 10d). The correlation of the vertical transverse component ρ (q_{tv}) in the anisotropic case shows good agreement between MC analyses and first-order approximation at least for $\sigma_Y^2 \leq 3$ (Figure 10f). The correlation of the horizontal transverse component ρ (q_{th}) derived from the MC analyses shows a less good agreement with the first-order approximations. Figure 10e shows that the negative correlations, in absolute terms, are small in the function of ρ (q_{th}) specially for higher σ_Y^2. Since the occurrence of the negative correlations in the correlograms of the transverse velocity components is a straightforward consequence of the continuity equation [see, e.g., *Rubin*, 2003] and therefore should be present, the following discussion is focused on that issue: In Figures 11a and 11b the ensemble correlogram is presented together with the ensemble indicator correlogram (cutoff = 0) for the cases $\sigma_Y^2 = 0.5$ and $\sigma_Y^2 = 3.0$ at $e = 0.017$. In the case $\sigma_Y^2 = 0.5$ both correlogram and indicator correlogram fit relatively well to the first-order approximation. In the case $\sigma_Y^2 = 3.0$ only the indicator correlogram shows a relatively good fit to the first-order approximation. It can be seen that the deviation between ensemble correlogram and ensemble indicator correlogram are relatively small for $\sigma_Y^2 = 0.5$, but obvious for $\sigma_Y^2 = 3.0$. Therefore the estimation of ρ (q_{th}) seems to be strongly depending on the nonnormality of the probability density distribution of q_{th}. In fact, the kurtosis of q_{th} increases at least by one order of magnitude with σ_Y^2 increasing from 0.5 to 3.0 (see section 4.1). We suggest that the extremely high and extremely low values of q_{th} in the tailing of the very peak shaped probability density distribution with high kurtosis, destroy the spatial correlation structure of the flow velocity fields. As a consequence the correlations decrease more rapid with the separation distance and the negative correlations, in absolute terms, are decreasing simultaneously. Moreover, Figure 11c shows clearly that the shape of the indicator correlograms are

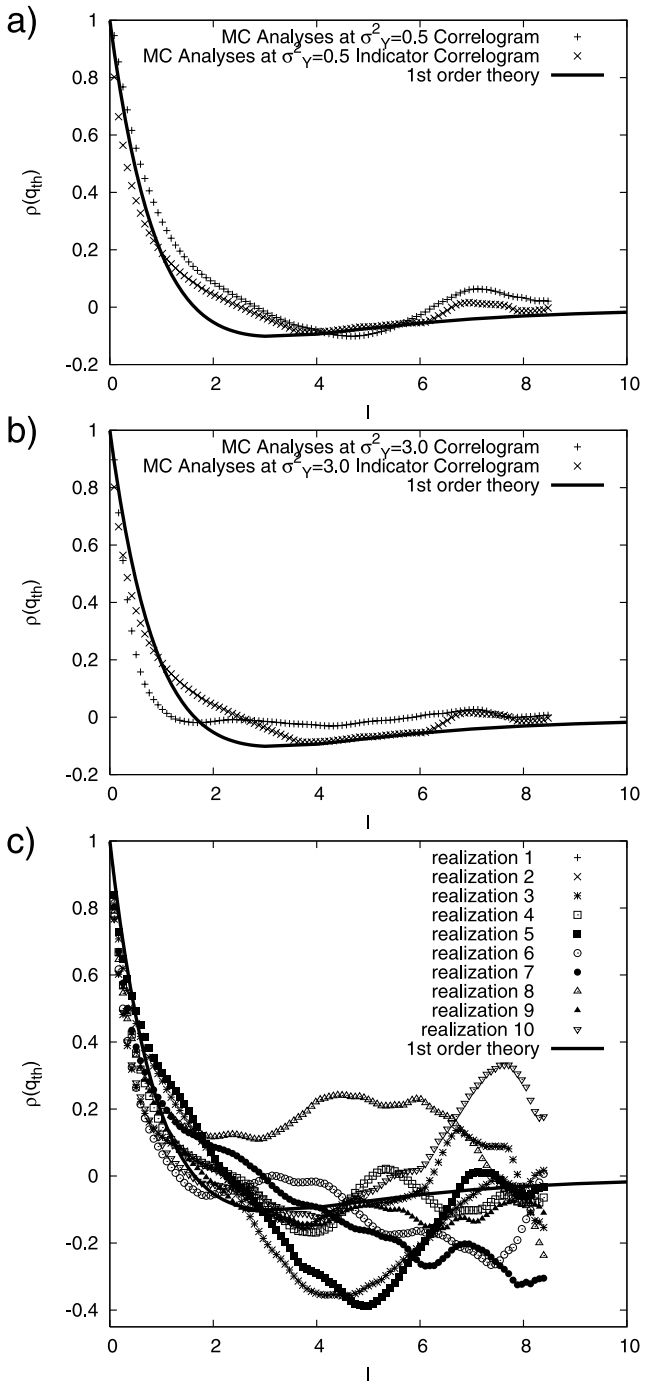

Figure 11. Estimated correlograms and indicator correlograms (cutoff = 0) of the transverse horizontal velocity component in the longitudinal direction for different variances of the logarithm of the hydraulic conductivity in a strongly anisotropic case ($e = 0.017$). Along the abscissa the normalized lag distance, $I = \xi/\lambda_h$, is applied. The ensemble correlograms and indicator correlograms are given for (a) $\sigma_Y^2 = 0.5$ and (b) $\sigma_Y^2 = 3.0$. (c) Indicator correlograms at $\sigma_Y^2 = 3.0$ for single realizations.

extremely variable comparing single realizations. Therefore it cannot be excluded that the correlograms are not statistically converged. We suggest that this is the reason for a nonperfect fit between the ensemble indicator correlogram and the first-order theory. To prove that, MC analyses including more realizations and larger domains are needed.

5. Summary and Conclusions

[54] High-resolution 3-D Monte Carlo analyses were conducted to derive velocity statistics for a range of variances of the logarithm of the hydraulic conductivity $0.5 \leq \sigma_Y^2 \leq 3.0$ and anisotropy ratios $0.017 \leq e \leq 1$. The statistical ensemble parameters of the generated hydraulic conductivity fields are in good accordance with the preset input parameters. The flow simulations showed small relative mass balance errors. The influence of boundary conditions on the velocity statistics was investigated in order to extract an inner core from the entire flow domain, in which the statistics of the velocity are unaffected by the boundary conditions. These statistics can then be compared with those of an infinite flow domain and consequently with those from approximated solutions of the stochastic flow equation. From the ensemble statistics, following conclusions can be drawn:

[55] 1. The MC analyses show that with increasing σ_Y^2 and increasing anisotropy the probability density function of q_l exhibits an increasing asymmetry with a tail to the right. The kurtosis increases simultaneously. The probability density functions of both transverse components show an increase of the kurtosis with increasing σ_Y^2 and increasing anisotropy.

[56] 2. The mean Darcy velocity, $\mu(q_l)$, increases with increasing σ_Y^2 and increasing anisotropy. This is fairly well predicted by using second-order approximations. This holds even for highly heterogeneous and strongly anisotropic hydraulic conductivity fields.

[57] 3. The variance of the longitudinal component of the Darcy velocity, $\sigma^2(q_l)$, increases with increasing σ_Y^2 and increasing anisotropy. For isotropic cases this is well predicted by the first-order approximation for $\sigma_Y^2 \leq 0.5$. For $0.5 \leq \sigma_Y^2 \leq 2.5$, $\sigma^2(q_l)$ is better predicted by the second-order approximation. For $\sigma_Y^2 \geq 2.5$ both the first- and second-order approximation underestimate $\sigma^2(q_l)$. For strongly anisotropic cases, $\sigma^2(q_l)$ is predicted fairly well for $\sigma_Y^2 \leq 1$ by the second-order approximation. For higher values of σ_Y^2 both the first- and second-order approximation underestimate $\sigma^2(q_l)$.

[58] 4. The variance of the transverse horizontal component of the Darcy velocity, $\sigma^2(q_{th})$, increases with increasing σ_Y^2, and increasing anisotropy ratio. The latter is restricted to relatively small σ_Y^2. For higher σ_Y^2, $\sigma^2(q_{th})$ is more or less constant with e. In the isotropic case the first-order approximations predict $\sigma^2(q_{th})$ fairly well for $\sigma_Y^2 \leq 0.5$. If σ_Y^2 increases, $\sigma^2(q_{th})$ derived from the MC analyses are larger than the first-order approximations, but converge toward the second-order approximation. At $\sigma_Y^2 = 3$, the second-order approximation fits the results from the MC analyses fairly well. In strongly anisotropic cases the first- and second-order approximations underestimate $\sigma^2(q_{th})$, even for small σ_Y^2.

[59] 5. The variance of the transverse vertical component of the Darcy velocity, $\sigma^2(q_{tv})$, increases with increasing σ_Y^2 and increasing anisotropy ratio. In the isotropic cases the behavior of $\sigma^2(q_{tv})$ is equivalent to the behavior of $\sigma^2(q_{th})$. In anisotropic cases where $\sigma_Y^2 = 0.5$, $\sigma^2(q_{tv})$ is better described by a first-order approximation. For higher

σ_Y^2, $\sigma^2(q_{tv})$ is fairly well predicted by the second-order approximation.

[60] 6. In isotropic cases the correlation of the longitudinal component of the Darcy velocity in longitudinal direction, $\rho(q_l)$, is predicted fairly well using the first-order approximation. The correlations of the transverse components of the Darcy velocity in longitudinal direction, $\rho(q_{th})$ and $\rho(q_{tv})$, are also fairly well predicted with the first-order approximation. Solely the phenomenon that the correlations decrease more rapidly with the separation distance and simultaneously the negative correlations, in absolute terms, are decreasing with increasing σ_Y^2 is not predicted by the first-order approximation.

[61] 7. In anisotropic cases up to $\sigma_Y^2 = 3.0$, $\rho(q_l)$ is fairly well predicted using the first-order approximation. The first-order approximation of $\rho(q_{th})$ and $\rho(q_{tv})$ is independent from σ_Y^2, whereas the MC analyses show a steeper decrease of the correlation with the separation distance and simultaneously a decrease of the negative correlations, in absolute terms, with increasing σ_Y^2. This is more pronounced for $\rho(q_{th})$ than for $\rho(q_{tv})$.

[62] 8. We assume the discrepancies between approximate solutions of the stochastic flow equation and the results of the MC analyses strongly depending on the nonnormality of the probability density distribution of the velocity. The deviation from a normal probability density distribution increases with increasing σ_Y^2 and anisotropy. This results in an increase of the kurtosis of the velocity by at least one order of magnitude. We suggest that the extremely high and low values of the velocity within the tailing of the very peak-shaped probability density distribution with high kurtosis, destroy the spatial correlation structure of the flow velocity fields and at the same time increase the variances of the velocity.

[63] Although the MC analyses concentrate on flow only the results in this study permit speculations regarding the prediction of transport parameters. *Chin and Wang* [1992] showed that in heterogeneous isotropic 3-D hydraulic conductivity fields the estimation of the longitudinal dispersivity were correct for at least $\sigma_Y^2 = 1.5$ using first-order theory. The transverse dispersivities are correct only for $\sigma_Y^2 = 0.5$. Higher σ_Y^2 lead to an underestimation of the transverse dispersivities. We suggest that the use of second-order approximations of the transverse dispersivities should lead to better estimations. In heterogeneous anisotropic 3-D hydraulic conductivity fields the estimation of the longitudinal macrodispersivity is valid up to $\sigma_Y^2 = 0.4$ and second-order approximations up to $\sigma_Y^2 = 0.6$ [*Naff et al.*, 1998b]. An increase of σ_Y^2 up to 0.9 shows increasing deviations between MC results and second-order approximation [*Naff et al.*, 1998b, Figure 4]. On the basis of the results of the present study we suggest a further increase of σ_Y^2 should lead to increasing underestimation of the longitudinal macrodispersivity.

[64] **Acknowledgments.** The authors thank the three unknown reviewers; their work enhanced the quality of this paper. Andreas Englert wishes to acknowledge the Deutsche Forschungsgemeinschaft (DFG) for financial support. We thank the Central Institute for Applied Mathematics (ZAM) within the Research Center Jülich and the John von Neumann Institute for Computing (NIC) for providing computation time on the Juelich Multi Processor (JUMP), but most of all for the permanent support using the JUMP. The authors are grateful to N. Suciu for fruitful discussions. They also acknowledge the technical assistance during the computations offered by H. Hardelauf and J. Heidbüchel.

References

Ababou, R., D. McLaughlin, L. W. Gelhar, and A. F. B. Tompson (1989), Numerical simulation of three-dimensional saturated flow in randomly heterogeneous porous media, *Transp. Porous Media*, *4*, 549–565.

Bellin, A., P. Salandin, and A. Rinaldo (1992), Simulation of dispersion in heterogeneous porous formations: Statistics, first-order theories, convergence of computations, *Water Resour. Res.*, *28*(9), 2211–2227.

Boggs, M. J., S. C. Young, L. M. Beard, L. W. Gelhar, K. R. Rehfeld, and E. E. Adams (1992), Field study of dispersion in a heterogeneous aquifer: 1. Overview and site description, *Water Resour. Res.*, *28*(12), 3281–3291.

Bonilla, F. A., and J. H. Cushman (2000), Role of boundary conditions in convergence and nonlocality of solutions to stochastic flow problems in bounded domains, *Water Resour. Res.*, *36*(4), 981–997.

Burr, D. T., E. A. Sudicky, and R. L. Naff (1994), Nonreactive and reactive solute transport in three-dimensional porous media: Mean displacement, plume spreading, and uncertainty, *Water Resour. Res.*, *30*(3), 791–815.

Chin, D. A., and T. Wang (1992), An investigation of the validity of first-order stochastic dispersion theories in isotropic porous media, *Water Resour. Res.*, *28*(6), 1531–1542.

Dagan, G. (1984), Solute transport in heterogeneous formations, *J. Fluid Mech.*, *145*, 151–177.

Dagan, G. (1989), *Flow and Transport in Porous Formations*, Springer, New York.

Deng, F. W., and J. H. Cushman (1995), On higher-order corrections to the flow velocity covariance, *Water Resour. Res.*, *31*(7), 1659–1672.

Deng, F. W., and J. H. Cushman (1998), Higher-order corrections to the flow velocity covariance tensor, revisited, *Water Resour. Res.*, *34*(1), 103–106.

Deutsch, C. V., and A. G. Journel (1998), *GSLIB: Geostatistical Software Library and User's Guide*, 2nd ed., Oxford Univ. Press, New York.

Dykaar, B. B., and P. K. Kitanidis (1992), Determination of the effective hydraulic conductivity for heterogeneous porous media using a numerical spectral approach: 2. Results, *Water Resour. Res.*, *28*(4), 1167–1178.

Englert, A., H. Hardelauf, J. Vanderborght, and H. Vereecken (2004), Numerical modelling of flow and transport on massively parallel computers, in *NIC Symposium 2004*, *NIC Publ. Ser.*, vol. 20, edited by D. Wolf, G. Münster, and M. Kremer, pp. 409–418, John von Neumann Inst. for Comput., Jülich, Germany.

Gelhar, L. W. (1993), *Stochastic Subsurface Hydrogeology*, Prentice-Hall, Upper Saddle River, N. J.

Gelhar, L. W., and C. L. Axness (1983), Three dimensional stochastic analysis of macrodispersion in aquifers, *Water Resour. Res.*, *19*(1), 161–180.

Hassan, A., J. H. Cushman, and J. W. Delleur (1998), A Monte Carlo assessment of Eulerian flow and transport perturbation models, *Water Resour. Res.*, *34*(5), 1143–1163.

Hsu, K. C., and S. P. Neuman (1997), Second-order expressions for velocity moments in two- and three-dimensional statistically anisotropic media, *Water Resour. Res.*, *33*(4), 625–637.

Hsu, K. C., D. Zhang, and S. P. Neuman (1996), Higher-order effects on flow and transport in randomly heterogeneous porous media, *Water Resour. Res.*, *32*(3), 571–582.

Janković, I., A. Fiori, and G. Dagan (2003a), Flow and transport in highly heterogeneous formations: 3. Numerical simulations and comparison with theoretical results, *Water Resour. Res.*, *39*(9), 1270, doi:10.1029/2002WR001721.

Janković, I., A. Fiori, and G. Dagan (2003b), Effective conductivity of an isotropic heterogeneous medium of lognormal conductivity distribution, *Multiscale Model. Simul.*, *1*(1), 40–56.

Kraichnan, R. H. (1970), Diffusion by a random velocity field, *Phys. Fluids*, *13*(1), 22–31.

Leblanc, D. R., S. P. Garabedian, K. M. Hess, L. W. Gelhar, R. D. Quadri, K. G. Stollenwerk, and W. W. Wood (1991), Large-scale natural gradient tracer test in sand and gravel, Cape Cod, Massachusetts: 1. Experimental design and observed tracer moment, *Water Resour. Res.*, *27*(5), 895–910.

Mackay, D. M., D. L. Freyberg, P. V. Roberts, and J. A. Cherry (1986), A natural gradient experiment on solute transport in a sand aquifer: 1. Approach and overview of plume movement, *Water Resour. Res.*, *22*(13), 2017–2029.

Matheron, G. (1967), *Elements Pour une Theorie des Millieux Poreux*, Masson et Cie, Paris.

Naff, R. L., D. F. Haley, and E. A. Sudicky (1998a), High-resolution Monte Carlo simulation of flow and conservative transport in heterogeneous porous media: 1. Methodology and flow results, *Water Resour. Res.*, *34*(4), 663–677.

Naff, R. L., D. F. Haley, and E. A. Sudicky (1998b), High-resolution Monte Carlo simulation of flow and conservative transport in heterogeneous porous media: 2. Transport results, *Water Resour. Res.*, *34*(4), 679–697.

Neuman, S. P., and S. Orr (1993), Prediction of steady state flow in nonuniform geologic media by conditional moments: Exact nonlocal formalism, effective conductivities, and weak approximation, *Water Resour. Res.*, *29*, 341–346.

Neuman, S. P., S. Orr, O. Levin, and E. Paleologos (1992), Theory and high-resolution finite elemente analysis of 2-D and 3-D effective permeabilities in strongly heterogeneous porous media, in *Mathematical Modeling in Water Resources*, vol. 2, edited by T. F. Russel et al., pp. 118–136, Elsevier, New York.

Oliver, L. D., and G. Christakos (1996), Boundary condition sensitivity analysis of the stochastic flow equation, *Adv. Water Resour.*, *19*(2), 109–120.

Rubin, Y. (2003), *Applied Stochastic Hydrogeology*, Oxford Univ. Press, New York.

Rubin, Y., and G. Dagan (1988), Stochastic analysis of boundaries effects on head spatial variability in heterogeneous aquifers: 1. Constant head boundary, *Water Resour. Res.*, *24*(10), 1689–1697.

Rubin, Y., and G. Dagan (1989), Stochastic analysis of boundaries effects on head spatial variability in heterogeneous aquifers: 2. Impervious boundary, *Water Resour. Res.*, *25*(4), 707–712.

Rubin, Y., and G. Dagan (1992), A note on head and velocity covariances in three-dimensional flow through heterogeneous anisotropic porous media, *Water Resour. Res.*, *28*(5), 1463–1470.

Russo, D. (1995), On the velocity covariance and transport modeling in heterogeneous anisotropic porous formations: 1. Saturated flow, *Water Resour. Res.*, *31*(1), 129–137.

Russo, D. (1998), A note on the velocity covariance and transport modeling in partially saturated heterogeneous porous formations of two- and three-dimensional structures, *Adv. Water Resour.*, *21*(3), 251–258.

Salandin, P., and V. Fiorotto (1998), Solute transport in highly heterogeneous aquifers, *Water Resour. Res.*, *34*(5), 949–961.

Seidemann, R. (1996), Parallelisierung eines Finite Elemente Programms zur Modellierung des Transports von Stoffen durch heterogene poröse Medien, Ph.D. thesis, Rheinische Friedrich-Wilhelms Univ. Bonn, Bonn, Germany.

Tompson, A. F. B., and L. W. Gelhar (1990), Numerical simulation of solute transport in three-dimensional, randomly heterogeneous porous media, *Water Resour. Res.*, *26*(10), 2541–2562.

Vereecken, H., G. Lindenmayr, O. Neuendorf, U. Döring, and R. Seidemann (1994), Trace a mathematical model for reactive transport in 3D variably saturated porous media, *Tech. Rep. KFA-ICG-4-501494*, Forsch. Jülich GmbH, Jülich, Germany.

Vereecken, H., U. Döring, H. Hardelauf, U. Jaekel, U. Hashagen, O. Neuendorf, H. Schwarze, and R. Seidemann (2000), Analysis of solute transport in heterogeneous aquifer: The Krauthausen field experiment, *J. Contam. Hydrol.*, *45*, 329–358.

Wonnacott, R. J., and T. H. Wonnacott (1985), *Introductary Statistics*, 4th ed., John Wiley, Hoboken, N. J.

Zhang, D. (2002), *Stochastic Methods for Flow in Porous Media: Coping With Uncertainties*, Elsevier, New York.

A. Englert, J. Vanderborght, and H. Vereecken, Agrosphere Institute (ICG IV), ICG, Research Center Jülich, D-52425 Jülich, Germany. (a.englert@fz-juelich.de)